Inorganic Chemistry
Forum Article

Inorg. Chem. **2010**, *49*, 6317–6329 **6317**
DOI: 10.1021/ic902157z

Mechanisms of Peroxynitrite Interactions with Heme Proteins

Jia Su and John T. Groves*

Department of Chemistry, Princeton University, Princeton, New Jersey 08544

Received November 1, 2009

Oxygenated heme proteins are known to react rapidly with nitric oxide (NO) to produce peroxynitrite (PN) at the heme site. This process could lead either to attenuation of the effects of NO or to nitrosative protein damage. PN is a powerful nitrating and oxidizing agent that has been implicated in a variety of cell injuries. Accordingly, it is important to delineate the nature and variety of reaction mechanisms of PN interactions with heme proteins. In this Forum, we survey the range of reactions of PN with heme proteins, with particular attention to myoglobin and cytochrome *c*. While these two proteins are textbook paradigms for oxygen binding and electron transfer, respectively, both have recently been shown to have other important functions that involve NO and PN. We have recently described direct evidence that ferrylmyolgobin (ferrylMb) and nitrogen dioxide (NO_2) are both produced during the reaction of PN and metmyolgobin (metMb) (Su, J.; Groves, J. T. *J. Am. Chem. Soc.* **2009**, *131*, 12979−12988). Kinetic evidence indicates that these products evolve from the initial formation of a caged radical intermediate [Fe^{IV}═O·NO_2]. This caged pair reacts mainly via internal return with a rate constant k_r to form metMb and nitrate in an oxygen-rebound scenario. Detectable amounts of ferrylMb are observed by stopped-flow spectrophotometry, appearing at a rate consistent with the rate, k_{obs}, of heme-mediated PN decomposition. Freely diffusing NO_2, which is liberated concomitantly from the radical pair (k_e), preferentially nitrates myoglobin Tyr103 and added fluorescein. For cytochrome *c*, Raman spectroscopy has revealed that a substantial fraction of cytochrome *c* converts to a β-sheet structure, at the expense of turns and helices at low pH (Balakrishnan, G.; Hu, Y.; Oyerinde, O. F.; Su, J.; Groves, J. T.; Spiro, T. G. *J. Am. Chem. Soc.*, **2007**, *129*, 504−505). It is proposed that a short β-sheet segment, comprising residues 37−39 and 58−61, extends itself into the large 37−61 loop when the latter is destabilized by protonation of H26, which forms an anchoring hydrogen bond to loop residue P44. This conformation change ruptures the Met80−Fe bond, as revealed by changes in ligation-sensitive Raman bands. It also induces peroxidase activity with the same temperature profile. This process is suggested to model the apoptotic peroxidation of cardiolipin by cytochrome *c*.

Introduction

Biochemistry of Peroxynitrite. This Forum, with its focus on nitric oxide, provides an opportunity to review the roles of reactive oxygen and nitrogen species and the variety of interactions of these species with metalloproteins. Hydrogen peroxide, superoxide ion, nitric oxide, nitrogen dioxide, and peroxynitrite ion all react with biological target molecules. Some of these interactions are carefully orchestrated aspects of signaling events within and among cells, others are part of the cell-killing machinery of the immune system, and some are pathological events and may lie at the root of many diseases. Metalloproteins can be altered with loss or gain of function as a result of these small reactive molecules. DNA can be cleaved, and lipid components can be oxidized or nitrated. The interactions of these species with each other can be sensed by the cell, resulting in a variety of responses including gene regulation and transcription. Indeed, there is accumulating evidence that the molecular dance of reactive oxygen and nitrogen species is central to the life and death cellular decisions in homeostasis or the initiation of apoptosis. New families of metallopharmaceuticals are emerging that serve both to probe the nature and mechanisms of these events and to affect the outcome. It is with this perspective that we look at the mechanisms of heme protein interaction with the biological oxidant peroxynitrite anion ($ONOO^-$) and its conjugate acid, peroxynitrous acid (ONOOH).

The formation of peroxynitrite (PN) within cells and tissue from the reaction of cellular nitric oxide (NO) with the superoxide radical was first proposed by Beckman nearly 2 decades ago. Since then, PN has become the focus of intense research alongside the development of NO chemistry. PN is a powerful nitrating and oxidizing agent. PN is produced by the reaction of NO and a superoxide ($O_2^{\bullet -}$) ion at diffusion-controlled rates ($\sim 1 \times 10^{10}$ M^{-1} s^{-1}).[1,2] The superoxide ion is both a

*To whom correspondence should be addressed. E-mail: jtgroves@Princeton.edu. Phone: (609) 258-3593. Fax: (609) 258-0348.

(1) Beckman, J. S.; Beckman, T. W.; Chen, J.; Marshall, P. A.; Freeman, B. A. *Proc. Natl. Acad. Sci. U.S.A.* **1990**, *87*, 1620–1624.

Published on Web 07/12/2010

byproduct of respiration and a component of the immune defense.[3] Under normal physiological conditions, the superoxide ion will be intercepted by superoxide dismutases (SODs). However, when NO concentrations reach ~10 μM in the vicinity of activated phagocytes, the target flux for $^{\bullet}NO$ with $O_2^{\bullet-}$ becomes ~10^5 s^{-1}, which is greater than that estimated for SOD (2.3×10^4 s^{-1}). Thus, under such conditions, the combination of $^{\bullet}NO$ with $O_2^{\bullet-}$ becomes competitive with the dismutation of $O_2^{\bullet-}$ by SODs and affords PN. The signature events of PN production within cells are protein and lipid nitrations, and these have been found to be an early event in the etiology of a variety of pathologies.

The sites of PN formation are assumed to be spatially associated with the source of superoxide, such as the plasma NADPH oxidases or the mitochondrial respiratory complexes. This insight derives from the fact that $O_2^{\bullet-}$ is also a short-lived radical. Moreover, superoxide has restricted diffusion across membranes because of the low pK_a (4.7) of the conjugate acid, the hydroperoxyl radical ($HO_2^{\bullet}$). Superoxide can be generated from two major sources: phagocytic NADPH oxidase (NOX)[4] and a mitochondrial respiratory chain.[5] Activated NOXs in phagocytes of various tissues assemble in membranes and reduce oxygen to superoxide. This generation of superoxide by NOXs is vital for effective host defense but also affords a pathway to form PN by combining with NO produced by the inflammatory cells.[2,6] Superoxide produced by complexes I and III in the mitochondrial electron transport chain is released asymmetrically to both sides of the mitochondrial inner membrane with different roles in these subcellular environments.[5] By contrast, NO is highly diffusive and relatively stable (the diffusion coefficient of NO has been reported to be 3300 μm^2 s^{-1}).[7] Although PN has not been directly detected in vivo, analytical methods are improving[8] and numerous diagnostic footprints of PN formation have been found in a variety of cell types, including macrophages,[9] neutrophils,[10,11] and cultured endothelial cells.[12,13] All of these cell types can generate NO concurrently with superoxide.

PN anion exists in equilibrium with its protonated form, peroxynitrous acid, with a pK_a of 6.8.[14] A summary of the reactions of PN is presented in Figure 1. The rates of PN production in specific compartments have been estimated to be as high as 50−100 μM min^{-1} in vivo.[15] The steady-state PN concentrations are estimated to be in the nanomolar range.[16,17] Another important feature of PN is its ability to diffuse readily across lipid membranes.[18] The calculated permeability coefficient for PN is 8.0×10^{-4} cm s^{-1}, which is comparable to that of H_2O and is approximately 400 times greater than that of superoxide. This high permeability means that, once formed, PN can diffuse a distance larger than the diameter of a typical cell, a characteristic that makes PN an extremely effective oxidant in executing damage even far from its origin. Thus, the reaction of NO with $O_2^{\bullet-}$ creates a highly transportable and highly reactive oxidant. In vitro experiments have shown oxidation of thiols, sulfides, transition-metal centers, ascorbate, olefins, benzene, phenols, and other aromatics by PN; these reactions have been thoroughly discussed in a recent review.[19] Moreover, PN exhibits a wide range of reactivity that results in the modification of many cellular targets. These modifications to enzymes, cellular DNA, and lipids often lead to loss of enzyme activity and damage to the integrity of DNA and cell membranes (Figure 1). Damage to DNA and lipids can eventually lead to cellular apoptosis.[20−22]

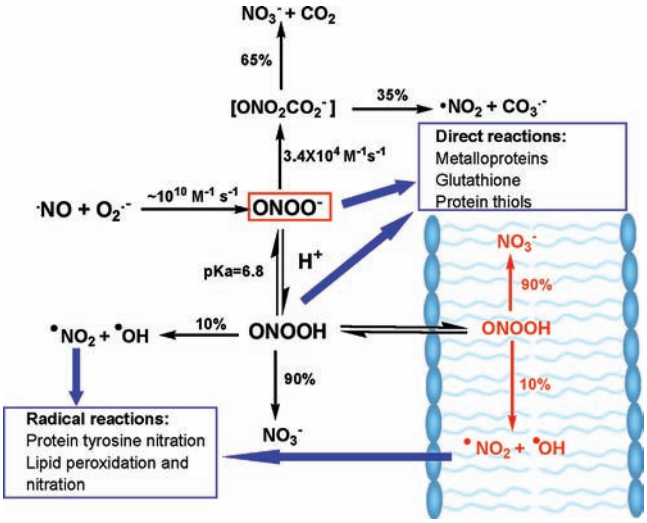

Figure 1. Reactions of PN in aqueous and lipid phases. Modified from ref 35.

Significantly, PN can induce post-translational modifications of proteins through nitration of tyrosine, oxidation of methionine, and nitrosylation of cysteine residues.[23,24] Tyrosine nitration has been detected in vivo in a large number of proteins during development,

(2) Ferrer-Sueta, G.; Radi, R. *ACS Chem. Biol.* **2009**, *4*, 161–177.
(3) Beckman, J. S.; Koppenol, W. H. *Am. J. Physiol.* **1996**, *271*, C1424–C1437.
(4) Lambeth, J. D. *Nat. Rev. Immunol.* **2004**, *4*, 181–189.
(5) Brand, M. D.; Affourtit, C.; Esteves, T. C.; Green, K.; Lambert, A. J.; Miwa, S.; Pakay, J. L.; Parker, N. *Free Radical Biol. Med.* **2004**, *37*, 755–767.
(6) Winterbourn, C. C. *Nat. Chem. Biol.* **2008**, *4*, 278–286.
(7) Malinski, T.; Taha, Z.; Grunfeld, S.; Patton, S.; Kapturczak, M.; Tomboulian, P. *Biochem. Biophys. Res. Commun.* **1993**, *193*, 1076–1082.
(8) Tiscornia, A.; Cairoli, E.; Marquez, M.; Denicola, A.; Pritsch, O.; Cayota, A. *J. Immunol. Methods* **2009**, *342*, 49–57.
(9) Ischiropoulos, H.; Zhu, L.; Beckman, J. S. *Arch. Biochem. Biophys.* **1992**, *298*, 446–451.
(10) Carreras, M. C.; Pargament, G. A.; Catz, S. D.; Poderoso, J. J.; Boveris, A. *FEBS Lett.* **1994**, *341*, 65–68.
(11) Rohn, T. T.; Nelson, L. K.; Sipes, K. M.; Swain, S. D.; Jutila, K. L.; Quinn, M. T. *J. Leukocyte Biol.* **1999**, *65*, 59–70.
(12) Mayer, B.; Schrammel, A.; Klatt, P.; Koesling, D.; Schmidt, K. *J. Biol. Chem.* **1995**, *270*, 17355–17360.
(13) Radi, R.; Peluffo, G.; Alvarez, M. N.; Naviliat, M.; Cayota, A. *Free Radical Biol. Med.* **2001**, *30*, 463–488.
(14) Radi, R.; Beckman, J. S.; Bush, K. M.; Freeman, B. A. *J. Biol. Chem.* **1991**, *266*, 4244–4250.
(15) Alvarez, M. N.; Piacenza, L.; Irigoin, F.; Peluffo, G.; Radi, R. *Arch. Biochem. Biophys.* **2004**, *432*, 222–232.
(16) Nalwaya, N.; Deen, W. M. *Chem. Res. Toxicol.* **2005**, *18*, 486–493.
(17) Quijano, C.; Romero, N.; Radi, R. *Free Radical Biol. Med.* **2005**, *39*, 728–741.
(18) Marla, S. S.; Lee, J.; Groves, J. T. *Proc. Natl. Acad. Sci. U.S.A.* **1997**, *94*, 14243–14248.
(19) Szabo, C. *Toxicol. Lett.* **2003**, *140−141*, 105–112.
(20) Burney, S.; Niles, J. C.; Dedon, P. C.; Tannenbaum, S. R. *Chem. Res. Toxicol.* **1999**, *12*, 513–520.
(21) Burney, S.; Caulfield, J. L.; Niles, J. C.; Wishnok, J. S.; Tannenbaum, S. R. *Mutat. Res.* **1999**, *424*, 37–49.
(22) Radi, R.; Cassina, A.; Hodara, R.; Quijano, C.; Castro, L. *Free Radical Biol. Med.* **2002**, *33*, 1451–1464.
(23) Goldstein, S.; Merenyi, G. *Methods Enzynol.* **2008**, *436*, 49−61.
(24) Landino, L. M. *Methods Enzymol.* **2008**, *440*, 95–109.

oxidative stress, and aging.[25] Proteomic methods have been utilized to identify specific protein nitration targets both in vivo and in cell culture models. For example, Stuehr et al. identified more than 40 nitrotyrosine-immunopositive proteins[26] in inflammatory cell models; Castenga et al.[27] applied proteomic approaches to determine specific targets of protein oxidation in brains suffering from Alzheimer's disease and successfully identified six protein targets.

Among protein targets in vivo, metalloproteins are particularly sensitive to the impairments induced by PN. As early as 1992, Ischiropoulos et al. found that bovine Cu/Zn SOD reacts with PN to form a stable, yellow protein-bound adduct identified as nitrotyrosine.[28] Zou and Ullrich later showed that prostacyclin synthase, a heme thiolate enzyme essential for the regulation of vascular tone, is nitrated and inactivated by submicromolar concentrations of PN.[29] Daiber et al. reported findings for NADH-NO reductase ($P450_{NOR}$) showing that reaction with PN can effectively catalyze phenol nitration without attacking its own tyrosine residues, whereas $P450_{BM3}$ undergoes self-nitration as well as phenol nitration.[30,31] The mitochondrial electron-transfer protein cytochrome *c* displays significant changes in redox properties upon nitration.[32,33] Tyrosine hydroxylase (a nonheme iron protein), which is the initial and rate-limiting enzyme in the biosynthesis of dopamine, is also inactivated by PN via tyrosine nitration and cysteine modification.[34]

The biochemistry and pathophysiology of PN have been thoroughly reviewed.[2,23,35−37] In this Forum, we present a discussion regarding the chemical mechanisms of heme protein/PN reactions, with particular attention to myoglobin, cytochrome P450, and cytochrome *c*.

Interaction of PN with Heme Proteins. Myoglobin (Mb) and Hemoglobin (Hb). Mb and Hb are best known for their oxygen storage and transport functions.[38] In the past decade, the idea that Mb and Hb may function as scavengers of reactive nitrogen species, such as NO, has been a subject of great interest. It has been recently realized that Mb is an efficient intracellular scavenger of NO, regulating NO homeostasis in the cardiac and skeletal muscles and thereby protecting mitochondrial respiration.[39] This novel function of Mb is based on the rapid and irreversible reaction of ferrous-oxygenated Mb (oxyMb) with NO, yielding ferric-oxidized Mb (metMb) and nitrate (NO_3^-).[40−42] The detailed mechanism of this process has not yet been fully elucidated, but it is clear that the complexity and importance of the Mb/NO interaction continues to develop. Indeed, the overexpression of Mb has recently been shown to be an early event in the etiology of epithelial cancers.[43] oxyHb was found to bind NO and form nitrosylated thiols.[44]

Scheme 1. Mechanisms for metMb-Catalyzed Decomposition of PN

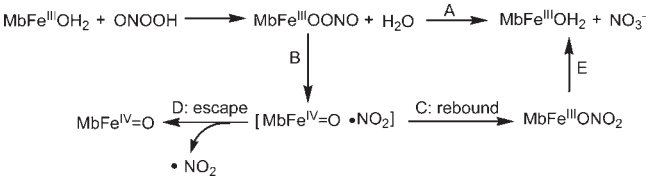

The ferric forms of Hb and Mb have been shown to *catalyze* the isomerization of PN to NO_3^-.[45−48] The catalytic rate constant determined by our group at pH 7.6 and 25 °C for metMb is ca. 1.0×10^4 M^{-1} s^{-1}.[45] Herold and Shivashankar measured the k_{cat} of metMb to be 7.7×10^4 M^{-1} s^{-1} at pH 7.0 and 20 °C.[49] The pH dependence of the catalytic rate constants indicates that HOONO is the species that reacts with the Fe^{III} center of the proteins. Two mechanisms regarding metMb/PN have been proposed, as summarized in Scheme 1. In both mechanisms, the first step is initiated by replacing the sixth ligand H_2O by HOONO, forming a transient intermediate MbFe^{III}OONO.[50] Electron paramagnetic resonance and UV−vis data possibly supporting MbFe^{III}OONO as the intermediate of the reaction of NO with oxyMb at alkaline pH have been presented.[40,51,52] However, because the MbFe^{III}OONO complex could not be detected at neutral pH, it probably decays to other intermediates at a very fast rate. Indeed, Raman[41] and kinetic data (vide infra)[53] have supported an alternative nitratoiron(III) formulation for the observed transient species, supporting a very rapid O−O bond cleavage in MbFe^{III}OONO.

(25) Bartesaghi, S.; Ferrer-Sueta, G.; Peluffo, G.; Valez, V.; Zhang, H.; Kalyanaraman, B.; Radi, R. *Amino Acids* **2007**, *32*, 501–515.
(26) Aulak, K. S.; Miyagi, M.; Yan, L.; West, K. A.; Massillon, D.; Crabb, J. W.; Stuehr, D. J. *Proc. Natl. Acad. Sci. U.S.A.* **2001**, *98*, 12056–12061.
(27) Castegna, A.; Thongboonkerd, V.; Klein, J. B.; Lynn, B.; Markesbery, W. R.; Butterfield, D. A. *J. Neurochem.* **2003**, *85*, 1394–1401.
(28) Ischiropoulos, H.; Zhu, L.; Chen, J.; Tsai, M.; Martin, J. C.; Smith, C. D.; Beckman, J. S. *Arch. Biochem. Biophys.* **1992**, *298*, 431–437.
(29) Zou, M. H.; Ullrich, V. *FEBS Lett.* **1996**, *382*, 101–104.
(30) Daiber, A.; Herold, S.; Schoneich, C.; Namgaladze, D.; Peterson, J. A.; Ullrich, V. *Eur. J. Biochem.* **2000**, *267*, 6729–6739.
(31) Daiber, A.; Schoneich, C.; Schmidt, P.; Jung, C.; Ullrich, V. *J. Inorg. Biochem.* **2000**, *81*, 213–220.
(32) Cassina, A. M.; Hodara, R.; Souza, J. M.; Thomson, L.; Castro, L.; Ischiropoulos, H.; Freeman, B. A.; Radi, R. *J. Biol. Chem.* **2000**, *275*, 21409–21415.
(33) Batthyany, C.; Souza, J. M.; Duran, R.; Cassina, A.; Cervenansky, C.; Radi, R. *Biochemistry* **2005**, *44*, 8038–8046.
(34) Kuhn, D. M.; Sadidi, M.; Liu, X.; Kreipke, C.; Geddes, T.; Borges, C.; Watson, J. T. *J. Biol. Chem.* **2002**, *277*, 14336–14342.
(35) Szabo, C.; Ischiropoulos, H.; Radi, R. *Nat. Rev. Drug Discovery* **2007**, *6*, 662–680.
(36) Pacher, P.; Beckman, J. S.; Liaudet, L. *Physiol. Rev.* **2007**, *87*, 315–424.
(37) Groves, J. T. *Curr. Opin. Chem. Biol.* **1999**, *3*, 226–235.
(38) Rossifanelli, A.; Antonini, E.; Caputo, A. *Adv. Protein Chem.* **1964**, *19*, 73–222.
(39) Brunori, M. *Trends Biochem. Sci.* **2001**, *26*, 209–210.
(40) Herold, S.; Exner, M.; Nauser, T. *Biochemistry* **2001**, *40*, 3385–3395.
(41) Yukl, E. T.; de Vries, S.; Moenne-Loccoz, P. *J. Am. Chem. Soc.* **2009**, *131*, 7234–7235.
(42) Doyle, M. P.; Hoekstra, J. W. *J. Inorg. Biochem.* **1981**, *14*, 351–358.
(43) Flonta, S. E.; Arena, S.; Pisacane, A.; Michieli, P.; Bardelli, A. *Am. J. Pathol.* **2009**, *175*, 201–206.
(44) Gow, A. J.; Luchsinger, B. P.; Pawloski, J. R.; Singel, D. J.; Stamler, J. S. *Proc. Natl. Acad. Sci. U.S.A.* **1999**, *96*, 9027–9032.
(45) Bourassa, J. L.; Ives, E. P.; Marqueling, A. L.; Shimanovich, R.; Groves, J. T. *J. Am. Chem. Soc.* **2001**, *123*, 5142–5143.
(46) Herold, S.; Shivashankar, K.; Mehl, M. *Biochemistry* **2002**, *41*, 13460–13472.
(47) Gardner, P. R. *J. Inorg. Biochem.* **2005**, *99*, 247–266.
(48) Gardner, P. R.; Gardner, A. M.; Martin, L. A.; Salzman, A. L. *Proc. Natl. Acad. Sci. U.S.A.* **1998**, *95*, 10378–10383.
(49) Herold, S.; Shivashankar, K. *Biochemistry* **2003**, *42*, 14036–14046.
(50) Schopfer, M. P.; Mondal, B.; Lee, D.-H.; Sarjeant, A. A. N.; Karlin, K. D. *J. Am. Chem. Soc.* **2009**, *131*, 11304–11305.
(51) Herold, S. *FEBS Lett.* **1999**, *443*, 80–84.
(52) Olson, J. S.; Foley, E. W.; Rogge, C.; Tsai, A. L.; Doyle, M. P.; Lemon, D. D. *Free Radical Biol. Med.* **2004**, *36*, 685–697.
(53) Goldstein, S.; Merenyi, G.; Samuni, A. *J. Am. Chem. Soc.* **2004**, *126*, 15694–15701.

The mechanism describing $MbFe^{III}OONO$ decay proposed by Herold and Shivashankar proceeds by a direct rearrangement of $MbFe^{III}OONO$ and yields metMb and 100% NO_3^-.[46,49] Additionally, they estimated the rate constant of this process (A) in Scheme 1 to be $205 \pm 5\ s^{-1}$.[40] The other mechanism, proposed by our group, suggests the formation of a transient radical cage intermediate $[Fe^{IV}{=}O\cdot NO_2]$, followed by $\cdot NO_2$ cage escape (D) or rebound (C).[45] The early evidence favoring this idea was the observation of Mb nitration and the nitration of fluorescein. This is the key difference in the two processes because, in the latter, freely diffusing NO_2 will emerge from the encounter of NO with oxyMb. This mechanism will be confirmed and delineated in more detail below.

Goldstein et al. have reported measurements of the dissociation rate of NO_3^- from the nitrato complex $MbFe^{III}ONO_2$, which was generated by pulse radiolysis from the reaction of ferrylMb and NO_2.[53] The value for the rate constant was $190 \pm 20\ s^{-1}$ at pH 9.7 and 20 °C, which is virtually identical with the rate reported by Herold et al. for the assumed $MbFe^{III}ONOO$ decay.[40] This similarity implies that the observed decay of $MbFe^{III}OONO$ by Herold et al. actually comprises two fast steps: the first is the rapid conversion to $MbFe^{III}ONO_2$ via ferrylMb and NO_2 (C); the second one is the release of NO_3^- from $MbFe^{III}ONO_2$ (E). Accordingly, the putative $MbFe^{III}OONO$ intermediate probably has not yet been observed. Recent freeze−quench Raman data reported by Yukl et al. appear to support the nitratoiron(III) formulation of the observed intermediate.[41]

We have recently reported a detailed study of the PN/Mb reaction.[54] The central conclusions of that work were that a caged radical intermediate $[Fe^{IV}{=}O\cdot NO_2]$ is indeed formed from $MbFe^{III}ONOO$ during the metMb/PN interaction. This caged pair $[Fe^{IV}{=}O\cdot NO_2]$ mainly rebounds to form metMb and NO_3^- in an oxygen-rebound scenario, while freely diffusing $\cdot NO_2$ is liberated concomitantly from the radical pair and preferentially nitrates Tyr103 in horse heart Mb (Scheme 1, pathway D).

The key result was the direct observation of a UV−vis spectral transient characteristic of $MbFe^{IV}{=}O$ that appeared at a rate commensurate with the rate of the PN/Mb reaction (Figure 2). The data indicate a mechanism that involves rate-limiting O−O bond homolysis in a peroxynitritoiron(III) heme species ($MbFe^{III}OONO$) to afford a caged $[Fe^{IV}{=}O\cdot NO_2]$ intermediate (Scheme 1), as we had originally suggested in our initial report.[45] Overall, the process is analogous to the process that we have described for synthetic iron and manganese porphyrins.[55−57] The major pathway to close the catalytic cycle is cage collapse of $[Fe^{IV}{=}O\cdot NO_2]$ to form an iron(III) heme and NO_3^-, a process analogous to ferryl oxygen rebound to carbon radical intermediates.[58]

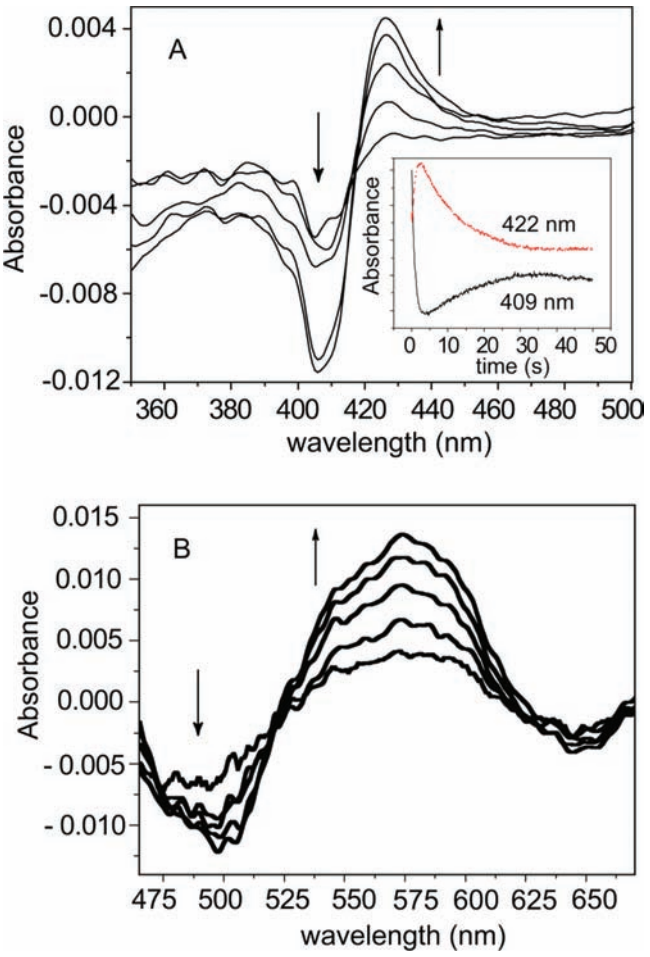

Figure 2. Direct spectroscopic detection of ferrylMb formation from the metMb and PN reaction, showing the (A) Soret and (B) Q-band regions (ref 54).

The results also show that $\cdot NO_2$ can diffuse away from the heme site to induce nitration elsewhere. To confirm this latter pathway, we employed fluorescein as a chemical trap of $\cdot NO_2$. The yield and kinetics of both ferrylMb and nitrofluorescein ($FlNO_2$) formation were used to quantitate the degree of dynamic cage escape of $\cdot NO_2$ into the protein interior and the medium during the catalytic decomposition of PN. Here the signature spectral changes upon nitration of fluorescein provide a very sensitive and informative measure of the flux of freely diffusing NO_2. As shown in Figure 3, the extent of NO_2 escape from the active site has a very large effect on the yield of fluorescein nitration. The data show that Mb catalyzes the nitration of fluorescein, with the initial rate of nitrofluorescein nitration increasing with the concentration of Mb. Kinetic simulations confirm the observed data, showing that (1) Mb accelerates the rate of fluorescein nitration in the early stages of the reaction and (2) the predicted yield of nitrofluorescein decreases much less than would be expected if all of NO_2 was captured by ferrylMb and converted to NO_3^-. Further, (3) the simulations reproduced the observed crossing of $[FlNO_2]$ versus time data plots at ~2.5 s for all concentrations of Mb. Significantly, all three of these features of the data are absent in simulations that did not allow for the cage escape of NO_2.

(54) Su, J.; Groves, J. T. *J. Am. Chem. Soc.* **2009**, *131*, 12979–12988.
(55) Lee, J. B.; Hunt, J. A.; Groves, J. T. *J. Am. Chem. Soc.* **1998**, *120*, 6053–6061.
(56) Lee, J. B.; Hunt, J. A.; Groves, J. T. *J. Am. Chem. Soc.* **1998**, *120*, 7493–7501.
(57) Shimanovich, R.; Groves, J. T. *Arch. Biochem. Biophys.* **2001**, *387*, 307–317.
(58) Groves, J. T. *Proc. Natl. Acad. Sci. U.S.A* **2003**, *100*, 3569–3574.

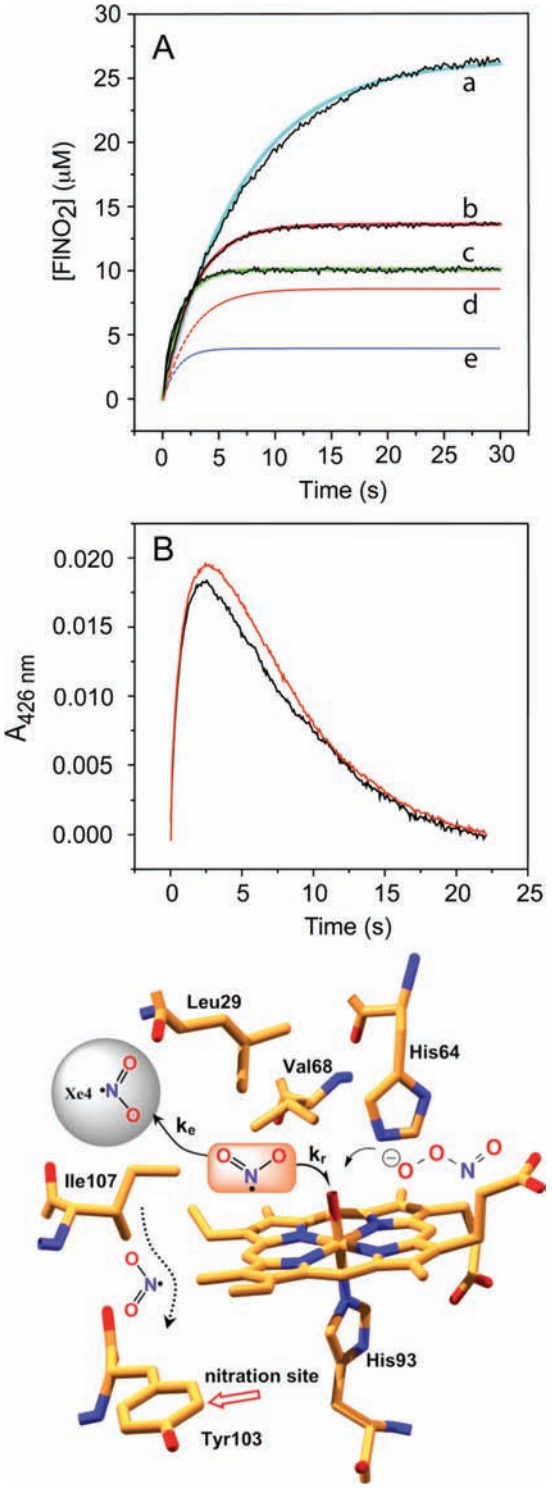

Figure 3. (A) Experimental and simulated time courses of nitrofluorescein formation. Experiments (E) and simulations (S) were done under the same reaction conditions: 30 μM fluorocein, 520 μM PN, and 0, 20, and 50 μM metMb. From top to bottom: 0 μM metMb (a, E in black and S in blue), 20 μM metMb (b, E in black and S in red), 50 μM metMb (c, E in black and S in green), 20 μM metMb with $k_e = 0\ s^{-1}$ (d, S as a dashed line and in red), and 50 μM metMb with $k_e = 0\ s^{-1}$ (e, S as a dashed line and in blue). (B) Formation and decay of ferrylMb during the reaction of 10 μM metMb and 100 μM PN in the absence (black) and presence (red) of 10 μM fluorescein. The structural figure illustrates the cage escape of NO_2 (ref 54).

Overall, the observed behavior of NO_2 within the internal Mb cavities is reminiscent of the recombination and escape scenarios observed for photodissociated O_2, NO, and CO and is further evidence of directed, small-molecule processing within the Mb structure.[59] The details of such diffusive cage phenomena within heme proteins have been extensively studied by photophysical techniques that allow the rapid formation of the dissociated heme−ligand intermediate and spectrophotometric monitoring of ligand rebinding.[60,61] For example, the kinetics of NO rebinding to deoxyMb have been shown to be biphasic. This feature of the data has been interpreted to be the result of a very rapid NO recombination from the distal pocket within 10 ps and a slower (200 ps) binding process of NO molecules from the xenon cavities.[62] Statistical mechanics simulations have shown that 5% of the NO molecules were still found in the distal pocket and xenon cavities even after 1 ns.[63] The kinetic barrier to this slower recombination phase has been associated with entropic considerations, solvent effects, and the dynamics of conformational gating for diffusive return to the distal pocket.[62,64,65]

The results for the reaction of Mb with PN indicate that an NO_2 capture and escape scenario also applies. The NO_2 formed at the active site by O−O bond homolysis in $MbFe^{III}OONO$ as the rate-limiting step can react with the ferryl oxygen to form NO_3^- (k_r). Overall, this is a one-electron oxidation of nitrogen with concomitant oxygen transfer from iron. In competition with this cage recombination, $\cdot NO_2$ can retreat into the protein interior (k_e). Moreover, Figure 3 illustrates that Tyr103 is preferentially nitrated, as was unambiguously determined from mass spectroscopic peptide sequence analysis on the purified mononitromyoglobin. This nitration selectivity is likely caused by the better solvent accessibility of this tyrosine as well as its coplanar donor-to-acceptor orientation with the heme.[66] Interestingly, the degree of cage escape of NO_2 observed for the Mb reaction is similar to the behavior of *alkyl*peroxynitrites upon rearrangement to alkyl nitrates.[67]

The extent of ferrylMb buildup and its time dependence can be understood in terms of a situation described by competitive cage collapse and cage escape (Scheme 2). The observed behavior reflects the balance between the oxidation rate k_1, the fraction of NO_2 cage escape $k_e/(k_e + k_r)$, and the reduction rate, k_3. The rates of the reaction cycle (k_1 and k_3) were measured directly.[45,54] Kinetic simulations of the measured rates and yields according to Scheme 2 showed about 10% cage escape of NO_2 ($k_e/k_r = 0.10$). ferrylMb can also be reduced by

(59) Frauenfelder, H.; McMahon, B. H.; Austin, R. H.; Chu, K.; Groves, J. T. *Proc. Natl. Acad. Sci. U.S.A.* **2001**, *98*, 2370–2374.
(60) Jongeward, K. A.; Magde, D.; Taube, D. J.; Marsters, J. C.; Traylor, T. G.; Sharma, V. S. *J. Am. Chem. Soc.* **1988**, *110*, 380–387.
(61) Austin, R. H.; Beeson, K. W.; Eisenstein, L.; Frauenfelder, H.; Gunsalus, I. C. *Biochemistry* **1975**, *14*, 5355–5373.
(62) Ionascu, D.; Gruia, F.; Ye, X.; Yu, A.; Rosca, F.; Beck, C.; Demidov, A.; Olson, J. S.; Champion, P. M. *J. Am. Chem. Soc.* **2005**, *127*, 16921–16934.
(63) Nutt, D. R.; Meuwly, M. *Biophys. J.* **2006**, *90*, 1191–1201.
(64) Goldbeck, R. A.; Bhaskaran, S.; Ortega, C.; Mendoza, J. L.; Olson, J. S.; Soman, J.; Kliger, D. S.; Esquerra, R. M. *Proc. Natl. Acad. Sci. U.S.A.* **2006**, *103*, 1254–1259.
(65) Frauenfelder, H.; McMahon, B. H.; Fenimore, P. W. *Proc. Natl. Acad. Sci. U.S.A.* **2003**, *100*, 8615–8617.
(66) Makinen, M. W.; Schichman, S. A.; Hill, S. C.; Gray, H. B. *Science* **1983**, *222*, 929–931.
(67) Goldstein, S.; Lind, J.; Merenyi, G. *J. Phys. Chem. A* **2004**, *108*, 1719–1725.

Scheme 2. Core Catalytic Cycle of metMb-Catalyzed PN Decay

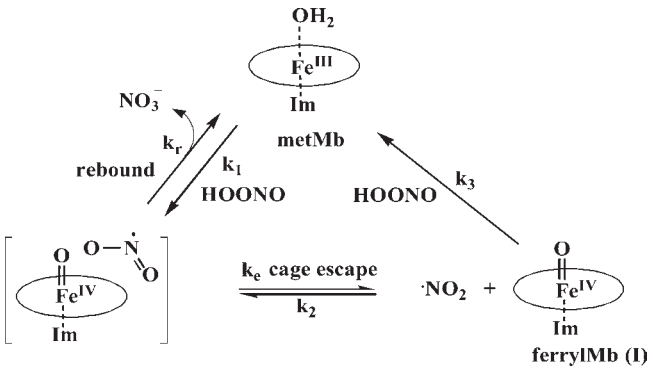

electron transfer from Tyr103[68] and reaction with freely diffusing NO_2 from the medium by a reencounter mechanism (k_2).[69]

The unambiguous observation of the ferrylMb intermediate provides strong confirmation of the proposed mechanism, in which the transient intermediate [Fe^{IV}=O·NO_2] can either proceed to cage escape or rebound to form NO_3^- and ferric Mb. The decomposition of PN catalyzed by water-soluble iron(III) porphyrins (e.g., FeTMPS and FeTMPyP) affords significant amounts of oxoiron(IV) porphyrins.[56,70] In particular, the fast rebound of NO_2 to Fe^{IV}TMPS accounts for an important pathway for Fe^{IV}=O reduction to Fe^{III}. The rate constant of this rebound can be as fast as 1.7×10^7 M^{-1} s^{-1}.[70]

Biological Implications. The results that we have described for the reaction of PN with metMb are pertinent to the discussion regarding the roles of oxyMb and oxyHb in trapping NO in vivo[52,71] because the two processes intersect at the Fe^{III}OONO intermediate. Recently, this *NO dioxygenase* activity has been extended to other Mb-like proteins, such as neuroglobin,[72] cytoglobin,[71] and bacterial hemoglobins.[73] One would expect, a priori, that ferrylMb and NO_2 would be formed to the same extent from the oxyMb/NO reaction as from metMb and PN. Olson and Gardner have described a thorough analysis of the isotopic content of NO_3^- resulting from the reaction of $^{18}O_2$-oxyMb with NO.[74] The results showed 99% dioxygenation of NO to afford $^{18}O_2$-^{16}O-nitrate via rebound to ferrylMb. Significantly, when we simulated the fate of ferrylMb and NO_2 formed from the single-turnover reaction of $^{18}O_2$-oxyMb with NO using the same kinetic scheme as that described above (Scheme 2) and the known rate constant for oxyMb + NO,[40] we also found only ~1% singly labeled NO_3^-, quantitatively consistent with the experimental result. The cage recombination mechanism affords little singly labeled NO_3^- in the oxyMb/NO reaction because the concentration of NO_2 is low under these conditions, making the bimolecular dimerization−hydrolysis pathway inefficient compared to NO_2 rebound and tyrosine nitration.

Theoretical Exploration of Heme Protein/PN Intermediates. As was seen from the preceding discussion, the goal of our dissection of the Mb/PN reaction has been to identify the major intermediates and measure the rates of the various transformations. Blomberg et al. studied the oxyMb/NO interaction using hybrid density functional theory (DFT).[75] They found that the free energy barrier to O−O bond cleavage in the Fe^{III}OONO intermediate for Mb was only 5.2 kcal mol^{-1} and formation of the [Fe^{IV}=O·NO_2] intermediate was exergonic by 6.6−11.2 kcal mol^{-1}, with the range depending on the entropy considerations. Oxygen rebound to form NO_3^- was found to be highly exergonic (−24.7 kcal mol^{-1}) with a negligible enthalpic barrier to capture of NO_2 by Fe^{IV}=O. The computed free-energy barrier to this NO_2 rebound was found to lie between 2.7 and 7.2 kcal mol^{-1}, depending on how the entropy of NO_2 was treated. The detection of ferrylMb and freely diffusing NO_2 suggests that the larger of the calculated exothermicities for NO_2 formation and the larger of the entropy barriers, both resulting from the more loosely bound NO_2, are closer to the real situation. Interestingly, Crespo et al. recently calculated the reaction energy (ΔE) of Fe^{III}OONO homolysis to Fe^{IV}=O and NO_2 as well as that of Fe^{IV}=O and NO_2 rebound to form $Fe^{III}ONO_2$ on the basis of a *Mycobacterium tuberculosis* truncated Hb model.[76] Both processes are exergonic. Combined with the analysis of spin and Mulliken populations, the Fe^{III}OONO complex was favorable to break homolytically into a Fe^{IV}=O and NO_2 pair. These calculations also show that the Fe^{IV}=O and ·NO_2 rebound reaction to form $Fe^{III}ONO_2$ (−18.0 kcal mol^{-1}) is much more exergonic than Fe^{III}OONO homolysis to Fe^{IV}=O and NO_2 (−8.1 kcal mol^{-1}), which implicates the dominance of the rebound pathway compared with the diffusion pathway. Thus, the experimental results that we have reported for the metMb/PN reaction are in remarkable agreement with the calculated reaction energy landscape.

In further analogy to this stochastic behavior of incipient radical pairs, we have recently shown that cage escape competes with cage recombination during the C−H bond hydroxylation reaction of the diiron hydroxylase AlkB.[77] The results suggest that caged radical pair phenomena may be more general in metalloenzyme catalysis. The realization here is that fluxional dynamics at the diiron active site can lead to a solvent-separated radical pair in the course of C−H hydroxylation (Scheme 3). Radical clock probes have revealed radical lifetimes in the range of 10−100 ps for cytochrome

(68) Lardinois, O. M.; Ortiz de Montellano, P. R. *Biochemistry* **2004**, *43*, 4601–4610.
(69) Goldstein, S.; Merenyi, G.; Samuni, A. *J. Am. Chem. Soc.* **2004**, *126*, 15694–15701.
(70) Shimanovich, R.; Hannah, S.; Lynch, V.; Gerasimchuk, N.; Mody, T. D.; Magda, D.; Sessler, J.; Groves, J. T. *J. Am. Chem. Soc.* **2001**, *123*, 3613–3614.
(71) Mammen, P. P.; White, J.; McGrath, A. J.; Kanatous, S. B.; Horton, J. W.; Garry, D. J. *Circulation* **2003**, *108*, 291–291.
(72) Brunori, M.; Giuffre, A.; Nienhaus, K.; Nienhaus, G. U.; Scandurra, F. M.; Vallone, B. *Proc. Natl. Acad. Sci. U.S.A.* **2005**, *102*, 8483–8488.
(73) Ascenzi, P.; Bocedi, A.; Bolognesi, M.; Fabozzi, G.; Milani, M.; Visca, P. *Biochem. Biophys. Res. Commun.* **2006**, *339*, 450–456.
(74) Gardner, P. R.; Gardner, A. M.; Brashear, W. T.; Suzuki, T.; Hvitved, A. N.; Setchell, K. D. R.; Olson, J. S. *J. Inorg. Biochem.* **2006**, *100*, 542–550.
(75) Blomberg, L. M.; Blomberg, M. R. A.; Siegbahn, P. E. M. *J. Biol. Inorg. Chem.* **2004**, *9*, 923–935.
(76) Crespo, A.; Marti, M. A.; Kalko, S. G.; Morreale, A.; Orozco, M.; Gelpi, J. L.; Luque, F. J.; Estrin, D. A. *J. Am. Chem. Soc.* **2005**, *127*, 4433–4444.
(77) Austin, R. N.; Luddy, K.; Erickson, K.; Pender-Cudlip, M.; Bertrand, E.; Deng, D.; Buzdygon, R. S.; van Beilen, J. B.; Groves, J. T. *Angew. Chem., Int. Ed.* **2008**, *47*, 5232–5234.

Scheme 3. Radical Cage Dynamics, with Cage Escape (k_e) from the Initial Radical Pair (RP) To Form a Solvent-Separated Radical Pair (RPss) Competing with Oxygen Rebound (k_r), That Provide a Precedented Explanation for the Facilitated Rearrangement of Some Radical Probes (ref 77)

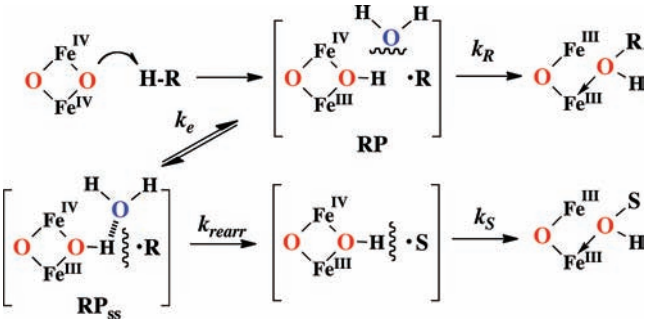

P450[78] to 10 ns for AlkB.[77] These longer lifetimes allow for significant motion of the intermediate radical within the substrate-binding cavity. Moreover, the kinetics of rapid, diffusional cage escape of the intermediate radical dictates that clock timing will be affected. In particular, slower radical clock probes may show as much or more rearrangement than faster clocks if cage escape for those radicals is competitive with rebound to form products. Indeed, exactly this situation occurs during hydroxylation of norcarane and bicyclohexane by AlkB. The radical rearrangement of the 2-norcaranyl radical is 10-fold faster than that of the 2-bicyclo[3.1.0]hexyl radical, yet almost 2-fold more rearrangement was observed for the slower probe. The lesson here is that while intermediate radicals formed during substrate hydroxylation can be detected by such diagnostic probes, one should not expect a strict ordering of the substrate rearrangement according to solution- or gas-phase rearrangement rates for those molecules.

Cytochrome P450, Prostaglandin Synthase, Chloroperoxidase, and PN. Thiolate-ligated heme proteins, including various cytochrome P450s (CYP), NO synthase (NOS), prostacyclin synthase (PGI_2), chloroperoxidase (CPO), etc., have been shown to interact with PN and to be inactivated by PN-mediated nitration. Importantly, these nitrated or nitroslyated heme proteins appear to be of pathological significance and are detected in Parkinson's and Alzheimer's diseases, neurodegenerative diseases, and cardiovascular disorders.[35]

Among the earliest observations of PN damage to heme proteins was the report by Zou and Ullrich of the PN-induced inactivation of PGI_2 synthase,[29] a thiolate-ligated heme protein involved in inflammatory response and platelet accumulation in humans. In subsequent work, they investigated the interactions and mechanisms of PN with $P450_{CAM}$, $P450_{NOR}$, CPO, microperoxidase (MP-11), and $P450_{BM3}$.[30,31,79,80] Combining stopped-flow experiments and phenol nitration results, it was concluded that a Fe^{IV}=O (compound II) species was a common intermediate in all five reactions via a mechanism

Scheme 4. Cytochrome P450 Cpd I Formation by LFP, Modified from Reference 83

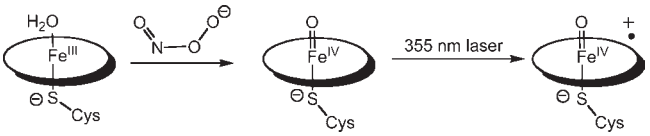

analogous to that of metMb (Scheme 1, paths B−E). Although the rate constants (k_{cat}) for these PN/P450 reactions were not reported, kinetic comparisons of PN decay in the presence of different heme proteins were carried out and showed a reactivity sequence of $P450_{NOR}$ > $P450_{BM3}$ > MP-11 > HRP (horseradish peroxidase).[80] Because k_{cat} for HRP was measured to be $\sim 10^6$ M^{-1} s^{-1}, k_{cat} of $P450_{NOR}$ and $P450_{BM3}$, though not determined, can be estimated to be around 10^7 M^{-1} s^{-1}.

Recently, identification and characterization of the P450/PN intermediates has stirred another wave of interest toward understanding the underlying mechanisms of P450/PN reactions. On the basis of the results from Ullrich[25,26] and Floris et al.,[81] it was believed that PN could be used to generate P450 compound II (Cpd II) in high yield and that under some conditions P450 Cpd II was more stable than CPO Cpd II. The reaction kinetics of CPO with PN were recently reported by Gebicka and Didik.[82] This paper reports CPO-*catalyzed* PN decay and the appearance of an intermediate, suggested to be CPO Cpd II on the basis of its visible spectrum in the Soret region, within 10 ms when 1 μM CPO was reacted with 10 μM PN at pH 5. The value of the bimolecular reaction rate of ferric CPO and PN was reported to be 10^7 M^{-1} s^{-1}, faster than the reaction with its natural substrate, hydrogen peroxide. The pH dependence of the decay rate indicated that, as with Mb, peroxynitrous acid, HOONO, was the reacting species. Interestingly, the authors reported that most of PN disappeared during the conversion of Cpd II back to ferric CPO. However, the three candidates to mediate the Cpd II reduction reaction ($\cdot NO_2$, nitrite ion, and PN) were not able to fully rationalize the whole process.[82]

Newcomb et al. have reported that the CPO/PN intermediate and a relatively stable CYP119/PN intermediate could serve as a platform from which to generate the elusive P450 compound I (Cpd I) by laser flash photolysis (LFP; Scheme 4).[83] The CPO/PN intermediate, with a Soret λ_{max} at 433 nm, arose and decayed within 400 ms, while the CYP119 species was longer lived, taking 40 s to decay. It was noted that decay of the CYP119/PN intermediate to the resting ferric protein was dependent upon the intensity of the spectrometer light beam. This CYP119 intermediate was assigned the Cpd II Fe^{IV}=O formulation. LFP of the intermediate led to another transient in about 5% conversion that had a less intense and blue-shifted Soret λ_{max} at ~400−410 nm and a weak Q band at 640−670 nm, typical of a porphyrin cation radical. The resting ferric protein absorbs at 417 nm. On this basis, the

(78) Austin, R. N.; Deng, D. Y.; Jiang, Y. Y.; Luddy, K.; van Beilen, J. B.; Ortiz de Montellano, P. R.; Groves, J. T. *Angew. Chem., Int. Ed.* **2006**, *45*, 8192–8194.
(79) Mehl, M.; Daiber, A.; Herold, S.; Shoun, H.; Ullrich, V. *Nitric Oxide* **1999**, *3*, 142–152.
(80) Zou, M. H.; Daiber, A.; Peterson, J. A.; Shoun, H.; Ullrich, V. *Arch. Biochem. Biophys.* **2000**, *376*, 149–155.
(81) Floris, R.; Piersma, S. R.; Yang, G.; Jones, P.; Wever, R. *Eur. J. Biochem.* **1993**, *215*, 767–775.
(82) Gebicka, L.; Didik, J. *J. Inorg. Biochem.* **2007**, *101*, 159–164.
(83) Newcomb, M.; Zhang, R.; Chandrasena, R. E. P.; Halgrimson, J. A.; Horner, J. H.; Makris, T. M.; Sligar, S. G. *J. Am. Chem. Soc.* **2006**, *128*, 4580–4581.

LFP intermediate was assigned as Cpd I of CYP119 with the usual oxoiron(IV) porphyrn cation radical formulation. Paradoxically, however, this intermediate was observed to be notably *unreactive* toward substrates, in surprising contrast to the known reactivity[83] of the well-characterized CPO Cpd I.[84−86]

Soon afterward, Green et al. reported results characterizing the $P450_{BM3}$/PN intermediate as an iron(III) nitrosyl ($Fe^{III}NO$) complex, not Fe^{IV}=O (or $Fe^{IV}OH$) on the basis of Mössbauer spectroscopy and supporting DFT calculations.[87] The Mössbauer sample was prepared by the freeze−quench technique, with the PN/$P450_{bm3}$ mixture being quenched after 450 ms. A critical piece of the experimental evidence for the $Fe^{III}NO$ assignment was the *diamagnetism* of the $P450_{BM3}$/PN intermediate. More recently, Newcomb et al. reported X-ray absorption spectroscopy (XAS) data of the CYP119/PN intermediate.[88] From a comparison of the results to XAS data for the authentic nitrosyl complex, they concluded that the CYP119/PN intermediate is a protonated ferryl, $Fe^{IV}OH$. This hydroxoiron(IV) porphyrin formulation had previously been found in Cpd II of CPO and P450s by Green et al.[89−91] It is to be noted that the Fe−N (NO) bond length of the authentic ferric nitrosyl and the Fe−O (OH) bond distance of the CYP119/PN intermediate were found to be the same (1.82 Å) from extended X-ray absorption fine structure data. Further, the Fe−S-(thiolate) distances of both species were also the same (2.24 Å). There was, however, a discernible difference in the X-ray absorption near-edge structure features of the two samples. While such a long Fe−X bond distance is expected for $Fe^{IV}OH$, ferric nitrosyls typically have much shorter Fe^{III}−N(NO) bond distances.[92,93] Kinetic studies of the decomposition of PN-generated CYP119 Cpd II were reported under conditions where the nitrosyl complex is apparently stable. P450 ferric nitrosyls are unstable to air, however, and some modes of PN decomposition afford oxygen. Newcomb et al. offer an explanation for the discrepancy between the two laboratories' observations. Nitrite, which is a contaminant in all PN solutions, was reported to react with the ferric CYP119 protein to form the nitrosyl over a period of 100 s. This, however, appears to be much longer than the 450 ms mixing time in the method described for the formation of the $P450_{BM3}$ ferric nitrosyl from PN reported by Green et al.[87] So, this issue appears not to be resolved. In the most recent reports, Newcomb et al. described the formation of CYP119 Cpd I in high conversion, also via LFP of the CYP119/PN intermediate.[94,95] Now, however, Cpd I is reactive toward substrates but has a spectrum very much like that of the resting ferric protein. Clearly, there is much more to do to characterize the spectral transients in these P450 reactions. On balance, the consensus view that P450 Cpd I is a particularly reactive, thiolate-ligated, oxoiron(IV) porphyrin cation radical similar to Cpd I of CPO appears to be correct.[96−99]

It is particularly pertinent in this regard that a highly reactive Cpd I model compound has recently been described in our laboratories.[100] The UV−vis spectral features of this intermediate, which include a broad, long-wavelength absorbance, indicate that it is an oxoiron(IV) porphyrin cation radical. Key to the observation of this species was the use of a water-soluble porphyrin with 4-*N*-methylpyridinium substituents on the meso positions. The results show that [OFe^{IV}-4-TMPyP$^+$] (**1**), which is accessed chemically from a peroxide precursor, is *orders of magnitude* more reactive than the well-studied tetramesityl analogues.[101−104] By mapping the rate constants observed for C−H bond cleavage by **1** onto the Brønsted−Evans−Polanyi relationship[105,106] for similar substrates, the bond dissociation energy (BDE) of HO-Fe^{IV}-4-TMPyP can be estimated to be ∼100 kcal mol^{-1} (Figure 4), much stronger than the values estimated for $HOFe^{IV}$TMP (92 kcal mol^{-1})[103] and $HOFe^{III}$TPFPP (∼86 kcal mol^{-1}).[107] The second-order rate constant for C−H bond cleavage in xanthene by this complex exceeded 10^6 $M^{-1}s^{-1}$, and **1** showed a rate constant for ethylbenzoic acid hydroxylation similar to that reported recently by Newcomb et al. for ethylbenzene with CYP119 and CPO Cpd I.[108]

An important advantage in this analysis was the finding that the reaction of Fe^{III}-4-TMPyP with *m*-chloroperoxybenzoic acid was very fast ($k_1 = 1.6 \times 10^7$ M^{-1} s^{-1}), affording a nearly complete conversion to **1** within 10 ms in the stopped-flow experiment (Scheme 5). An additional advantage was the clear and quantitative conversion of **1** to a relatively stable ferryl species ($k_2 = 8.8$ s^{-1}). The

(84) Davydov, R.; Osborne, R. L.; Kim, S. H.; Dawson, J. H.; Hoffman, B. M. *Biochemistry* **2008**, *47*, 5147–5155.
(85) Stone, K. L.; Behan, R. K.; Green, M. T. *Proc. Natl. Acad. Sci. U.S.A.* **2006**, *103*, 12307–12310.
(86) Stone, K. L.; Behan, R. K.; Green, M. T. *Proc. Natl. Acad. Sci. U.S.A.* **2005**, *102*, 16563–16565.
(87) Behan, R. K.; Hoffart, L. M.; Stone, K. L.; Krebs, C.; Green, M. T. *J. Am. Chem. Soc.* **2007**, *129*, 5855–5859.
(88) Newcomb, M.; Halgrimson, J. A.; Horner, J. H.; Wasinger, E. C.; Chen, L. X.; Sligar, S. G. *Proc. Natl. Acad. Sci. U.S.A.* **2008**, *105*, 8179–8184.
(89) Green, M. T.; Dawson, J. H.; Gray, H. B. *Science* **2004**, *304*, 1653–1656.
(90) Green, M. T. *Curr. Opin. Chem. Biol.* **2009**, *13*, 84–88.
(91) Behan, R. K.; Hoffart, L. M.; Stone, K. L.; Krebs, C.; Green, M. T. *J. Am. Chem. Soc.* **2006**, *128*, 11471–11474.
(92) Praneeth, V. K. K.; Paulat, F.; Berto, T. C.; George, S. D.; Nather, C.; Sulok, C. D.; Lehnert, N. *J. Am. Chem. Soc.* **2008**, *130*, 15288–15303.
(93) Ellison, M. K.; Scheidt, W. R. *J. Am. Chem. Soc.* **1999**, *121*, 5210–5219.
(94) Wang, Q.; Sheng, X.; Horner, J. H.; Newcomb, M. *J. Am. Chem. Soc.* **2009**, *131*, 10629–10636.
(95) Sheng, X.; Zhang, H. M.; Hollenberg, P. F.; Newcomb, M. *Biochemistry* **2009**, *48*, 1620–1627.
(96) Spolitak, T.; Dawson, J. H.; Ballou, D. P. *J. Biol. Chem.* **2005**, *280*, 20300–20309.
(97) Kellner, D. G.; Hung, S. C.; Weiss, K. E.; Sligar, S. G. *J. Biol. Chem.* **2002**, *277*, 9641–9644.
(98) Egawa, T.; Shimada, H.; Ishimura, Y. *Biochem. Biophys. Res. Commun.* **1994**, *201*, 1464–1469.
(99) Ortiz de Montellano, P. R. *Chem. Rev.* **2009**, *109*, ASAP DOI: 10.1021/cr9002193.
(100) Bell, S. R.; Groves, J. T. *J. Am. Chem. Soc.* **2009**, *131*, 9640–9641.
(101) Groves, J. T.; Watanabe, Y. *J. Am. Chem. Soc.* **1988**, *110*, 8443–8452.
(102) Groves, J. T.; Haushalter, R. C.; Nakamura, M.; Nemo, T. E.; Evans, B. J. *J. Am. Chem. Soc.* **1981**, *103*, 2884–2886.
(103) Pan, Z. Z.; Zhang, R.; Fung, L. W. M.; Newcomb, M. *Inorg. Chem.* **2007**, *46*, 1517–1519.
(104) Franke, A.; Fertinger, C.; van Eldik, R. *Angew. Chem., Int. Ed.* **2008**, *47*, 5238–5242.
(105) Mayer, J. M. *Acc. Chem. Res.* **1998**, *31*, 441–450.
(106) Shaik, S.; Kumar, D.; de Visser, S. P. *J. Am. Chem. Soc.* **2008**, *130*, 10128–10140.
(107) Jeong, Y. J.; Kang, Y.; Han, A. R.; Lee, Y. M.; Kotani, H.; Fukuzumi, S.; Nam, W. *Angew. Chem., Int. Ed.* **2008**, *47*, 7321–7324.
(108) Sheng, X.; Horner, J. H.; Newcomb, M. *J. Am. Chem. Soc.* **2008**, *130*, 13310–13320.

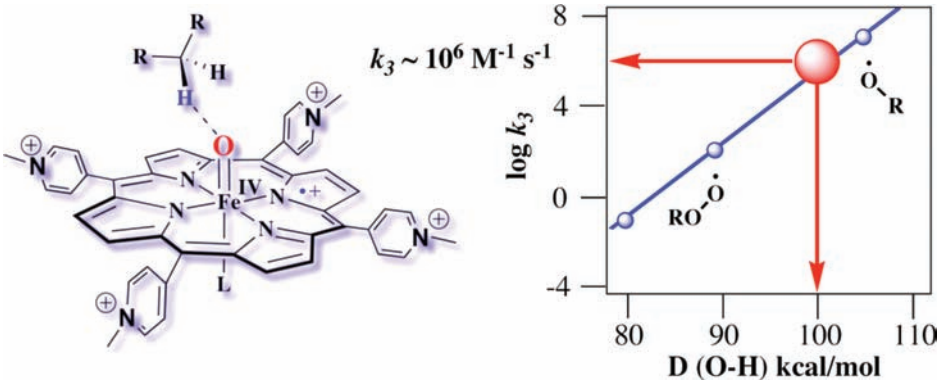

Figure 4. Rates of hydrogen abstraction by **1** revealing a 100 kcal mol^{-1} BDE for [H-OFe^{IV}-4-TMPyP^{+}] (ref 100).

Scheme 5. Kinetic Partitioning of **1** between the Spontaneous Decay to OFe^{IV}-4-TMPyP (k_2) and the Substrate Reaction (k_3) Resulting in the Formation of Fe^{III}-4-TMPyP

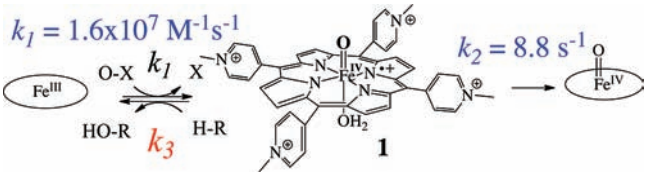

substrate reactivity could be assessed by measuring k_3 and by monitoring the ratio of Fe^{III} and Fe^{IV} species produced during the reaction using global analysis techniques.

It is of considerable interest to consider *why* **1** should be so reactive. Indeed, in a water solvent, one would expect the oxo-group lone pairs to be solvated with hydrogen bonds. The hydrogen abstraction transition state depicted in Figure 4 would require prior desolvation of the oxidant. We have shown that electron-withdrawing meso substituents dramatically *decrease* the reactivity of oxomanganese(V) porphyrins[109] because of stabilization of the singlet d^2 ground state with respect to the triplet and quintet manifolds, stabilization of the porphyrin HOMO, and the unique centrosymmetric *trans*-dioxo ligand arrangement.[110] Clearly, the situation for iron described here is markedly different. We have suggested that a relatively high redox potential for porphyrin ring oxidation for Fe^{III}-4-TMyP would destabilize the cation radical, making this Cpd I model compound a stronger oxidant. Further, efficient transmission of the electron deficit to the metal core is signaled by the low pK_a of the axial water in diaqua-Fe^{III}-4-TMyP (5.5), while the corresponding pK_a of diaqua-Fe^{III}TMPS is 7.5.[111] In this scenario, the high kinetic reactivity observed for **1** may result, in part, from a *decrease* of the energy level of the Fe $d_{x^2-y^2}$ orbital and spin-state-crossing phenomena into this orbital in the course of the reaction.[106,110,112−114] The results show that even subtle charge modulation surrounding the heme center of cytochrome P450 could result in a highly reactive P450 Cpd I.

Cytochrome *c*, PN, and Apoptosis. Cytochrome *c* (cyt *c*) is a small globular heme protein present at high concentrations (~1 mM) in the intermembrane space of mitochondria.[115] The primary role of cyt *c* is to shuttle electrons between respiratory complex III (cytochrome bc_1 complex) and complex IV (cytochrome *c* oxidase), where oxygen is reduced to water. However, possible alternative functions of cyt *c* have been recognized recently. Because cyt *c* is abundant in the mitochondrial intermembrane space, it is a potential target of the diffusible PN generated within or near the mitochondria. Cyt *c* nitration by PN in vitro was previously studied by Radi et al.[32,33] The direct reactivity of cyt c^{3+} with PN was not as pronounced as that of other heme proteins we have seen so far. The inactivity of cyt c^{3+} with PN can be attributed to the inaccessible heme cavity, which contains a six-coordinate heme iron. However, ferro cyt *c* is oxidized to ferri cyt *c* by PN with a reaction rate constant of 2.3×10^5 M^{-1} s^{-1}.[116] Significantly, the binding of cyt *c* to cardiolipin (CL), a unique phospholipid in the mitochondrial membranes, converts cyt *c* from a six-coordinate heme iron into a five-coordinate iron form[117−121] and thereby activates its interaction with PN via a metMb-like peroxidase mechanism.[54] Another intriguing *enzymatic* role for cyt *c* that has been suggested recently is its possible involvement in the biosynthesis of fatty

(109) Jin, N.; Groves, J. T. *J. Am. Chem. Soc.* **1999**, *121*, 2923–2924.
(110) De Angelis, F.; Jin, N.; Car, R.; Groves, J. T. *Inorg. Chem.* **2006**, *45*, 4268–4276.
(111) Shimanovich, R.; Groves, J. T. *Arch. Biochem. Biophys.* **2001**, *387*, 307–317.
(112) Balcells, D.; Raynaud, C.; Crabtree, R. H.; Eisenstein, O. *Inorg. Chem.* **2008**, *47*, 10090–10099.
(113) Altun, A.; Shaik, S.; Thiel, W. *J. Am. Chem. Soc.* **2007**, *129*, 8978–8987.
(114) Ogliaro, F.; de Visser, S. P.; Groves, J. T.; Shaik, S. *Angew. Chem., Int. Ed.* **2001**, *40*, 2874–2878.
(115) Vanneste, W. H. *Biochim. Biophys. Acta* **1966**, *113*, 175.
(116) Thomson, L.; Trujillo, M.; Telleri, R.; Radi, R. *Arch. Biochem. Biophys.* **1995**, *319*, 491–497.
(117) Kagan, V. E.; Tyurin, V. A.; Jiang, J.; Tyurina, Y. Y.; Ritov, V. B.; Amoscato, A. A.; Osipov, A. N.; Belikova, N. A.; Kapralov, A. A.; Kini, V.; Vlasova, I. I.; Zhao, Q.; Zou, M.; Di, P.; Svistunenko, D. A.; Kurnikov, I. V.; Borisenko, G. G. *Nat. Chem. Biol.* **2005**, *1*, 223–232.
(118) Kagan, V. E.; Bayir, H. A.; Belikova, N. A.; Kapralov, O.; Tyurina, Y. Y.; Tyurin, V. A.; Jiang, J. F.; Stoyanovsky, D. A.; Wipf, P.; Kochanek, P. M.; Greenberger, J. S.; Pitt, B.; Shvedova, A. A.; Borisenko, G. *Free Radical Biol. Med.* **2009**, *46*, 1439–1453.
(119) Kagan, V. E.; Bayir, A.; Bayir, H.; Stoyanovsky, D.; Borisenko, G. G.; Tyurina, Y. Y.; Wipf, P.; Atkinson, J.; Greenberger, J. S.; Chapkin, R. S.; Belikova, N. A. *Mol. Nutr. Food Res.* **2009**, *53*, 104–114.
(120) Jitkaew, S.; Witasp, E.; Zhang, S.; Kagan, V. E.; Fadeel, B. *J. Leukocyte Biol.* **2009**, *85*, 427–437.
(121) Godoy, L. C.; Munoz-Pinedo, C.; Castro, L.; Cardaci, S.; Schonhoff, C. M.; King, M.; Tortora, V.; Marin, M.; Miao, Q.; Jiang, J. F.; Kapralov, A.; Jemmerson, R.; Silkstone, G. G.; Patel, J. N.; Evans, J. E.; Wilson, M. T.; Green, D. R.; Kagan, V. E.; Radi, R.; Mannick, J. B. *Proc. Natl. Acad. Sci. U.S.A.* **2009**, *106*, 2653–2658.

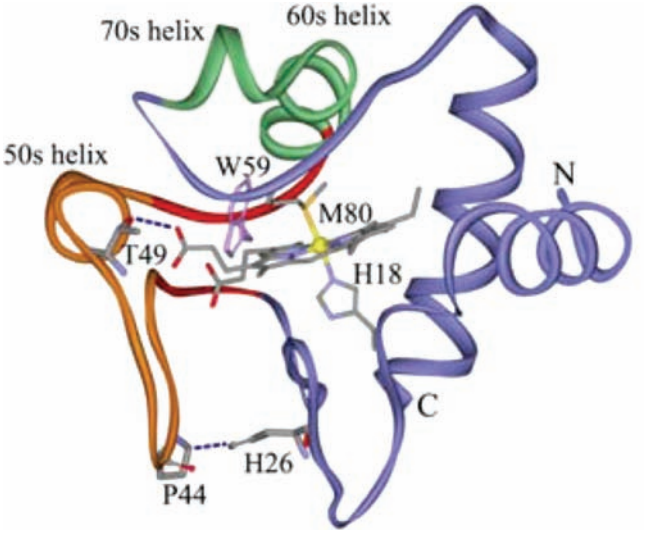

Figure 5. Ribbon diagram of cyt *c*, highlighting the 40s Ω loop (orange) and the 37−61 foldon with its 37−39/58−61 β-sheet neck (red). A conformational switch involving protonation of H26 and disruption of the H26···P44 hydrogen bond is proposed to displace the heme via the propionate hydrogen bonds, inducing Met80−Fe bond rupture (ref 125).

acid amides, which are now recognized as signaling molecules.[122−124]

Raman spectroscopy has revealed that a substantial fraction of cyt *c* converts to a β-sheet structure, at the expense of turns and helices at low pH.[125] It is proposed that a short β-sheet segment, comprising residues 37−39 and 58−61, extends itself into the large 37−61 loop when the latter is destabilized by protonation of H26, which forms an anchoring hydrogen bond to loop residue P44 (Figure 5). This conformation change ruptures the Met80−Fe bond, as revealed by changes in ligation-sensitive Raman bands. It also induces peroxidase activity with the same temperature profile. We found that peroxidase activity is indeed induced, with a T_m near 54 °C, when cyt *c* is heated at pH 3. Peroxidase activity was negligible at pH 7, regardless of the temperature. Thus, peroxidase activity and β-sheet formation are directly correlated. This process is suggested to model the apoptotic peroxidation of CL by cyt *c*.

We have studied the interactions of PN with a cyt *c*/liposome complex. In the presence of bovine heart CL (bhCL)-containing liposomes, cyt *c* was observed to catalyze PN decomposition. A linear dependence was observed for the rate of PN decay, $k_{obs} = k_{sp} + k_{cat}$[cyt *c*-CL]$_0$ (Figure 6A). The slope of k_{obs} vs [cyt *c*-bhCL] gave a k_{cat} value of 5.0×10^3 M^{-1} s^{-1} at pH 7.4 and 25 °C. In this set of experiments, the ratios of bhCL and cyt *c* were kept at 100:1, while the concentrations of cyt *c* and bhCL were varied simultaneously. The liposomes used in our experiments were composed of both CL and 1,2-dieleoyl-*sn*-glycero-3-phosphocholine (DOPC) (1:1); however, no catalysis of PN decomposition was seen when cyt *c* was mixed with liposomes that contained only DOPC (L/P = 200:1; Figure 6A). Clearly, the unique dianionic charge and four unsaturated fatty acid tails of CL cause this striking change of cyt *c* function.

To determine the nitration yields of cyt *c* in membranes, both aqueous and CL-associated reactions of cyt *c* (20 μM) with PN (1 mM) were carried out using the stopped-flow spectrometer as a mixing device. We first estimated the yields of nitrated cyt *c* in the absence of lipid vesicles by electrospray mass spectrometry (ESI-Q-TOF). The reaction of 20 μM cyt *c* with 1 mM PN resulted in (20 ± 3)% nitrated cyt *c*, as noted by a comparison of the peak areas corresponding to unreacted and modified peaks. In the presence of a physiological concentration of CO_2 (1.2 mM), the total nitration yield (including some dinitration) increased to (46 ± 6)%. Because lipid-bound cyt *c* solutions did not ionize well in the ESI source, cyt *c* tyrosine nitration yields in the presence of lipids were quantified by trypsin digestion followed by HPLC−MS/MS analysis (details are given in the Experimental Section). As seen in Figure 6B, when the ratio of cyt *c* and CL was 1:25, the nitrated tyrosine yield increased moderately from (20 ± 3)% to (26 ± 2)%. When the ratio of cyt *c* and CL increased to 1:100, the nitration yield enhanced dramatically to (45 ± 1)%, more than twice the amount observed in the absence of CL. By contrast, in the presence of only DOPC, the nitrotyrosine yield of cyt *c* was still ca. 20%. Interestingly, in the presence of 1.2 mM CO_2, the extent of nitration was always around 50%, whether CL was present or not.

In contrast to the inertness of native cyt *c* during PN decay, the bimolecular rate constant k_{cat} of bhCL-bound cyt *c* upon PN decay was measured to be 5000 M^{-1} s^{-1} (L/P = 100:1). This value is about half that of k_{cat} for metMb at pH 7.4 and 25 °C. Moreover, the nitration yields of cyt *c* by PN at a high bhCL/cyt *c* ratio of 100:1 were 2.5-fold higher than that of cyt *c* alone in an aqueous solution. It is therefore tempting to propose that bhCL-bound cyt *c* has been converted to an effective PN activator and catalyzes the formation of $\cdot NO_2$ via a metMb-like mechanism.[54] The presence of physiological concentrations of CO_2 (1.2 mM) in the bhCL/liposome solutions abolished the catalytic effect and resulted in ~50% nitration yields in all CO_2-containing samples. This observation is expected because PN reacts with CO_2 at a rate of 3×10^4 M^{-1} s^{-1},[126] 6 times faster than with the heme of cyt *c*. In the presence of 1.2 mM CO_2 and a 20 μM cyt *c*/CL complex (L/P = 100:1), over 90% PN flux would react with CO_2 and affords NO_2 and $CO_3^{\bullet-}$. Both radicals can nitrate tyrosine residues efficiently via tyrosyl radical formation. Hence, the catalysis of nitration by CO_2 outcompetes the one by the cyt *c*/bhCL complex, leading to almost identical yields of CO_2-involved cyt *c* nitration in both the absence and presence of CL. Additionally, the $CO_3^{\bullet-}$ anion radical is known to be impermeable to lipid membranes.[127]

Metalloporphyrins That Decompose PN. As mimics for metalloproteins, especially cytochrome P450s, water-soluble metalloporphyrin reactions with PN have been

(122) Zaccagnino, P.; Saltarella, M.; D'Oria, S.; Corcelli, A.; Saponetti, M. S.; Lorusso, M. *Free Radical Biol. Med.* **2009**, *47*, 585–592.
(123) Farrell, E. K.; Merkler, D. J. *Drug Discovery Today* **2008**, *13*, 558–568.
(124) Mueller, G. P.; Driscoll, W. J. *J. Biol. Chem.* **2007**, *282*, 22364–22369.
(125) Balakrishnan, G.; Hu, Y.; Oyerinde, O. F.; Su, J.; Groves, J. T.; Spiro, T. G. *J. Am. Chem. Soc.* **2007**, *129*, 504–505.
(126) Lymar, S. V.; Hurst, J. K. *J. Am. Chem. Soc.* **1995**, *117*, 8867–8868.
(127) Zhang, H.; Bhargava, K.; Keszler, A.; Feix, J.; Hogg, N.; Joseph, J.; Kalyanaraman, B. *J. Biol. Chem.* **2003**, *278*, 8969–8978.

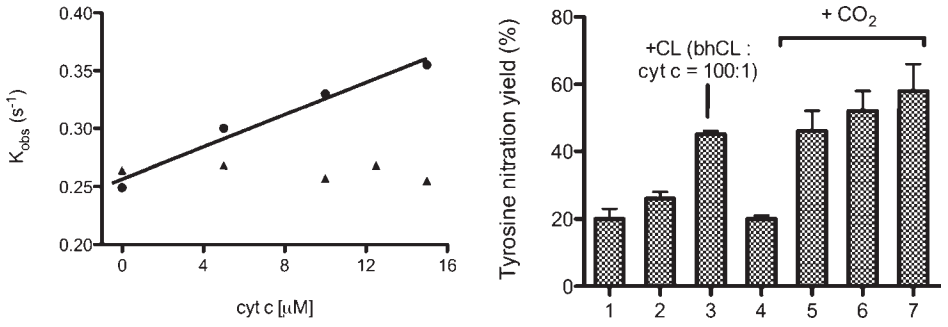

Figure 6. (A, left panel) Pseudo-first-order rate constants for the decay of PN vs the concentrations of cyt *c*/lipid complexes: (●) CL-containing liposomes (CL:DOPC = 1:1; CL:cyt *c* = 100:1); (▲) DOPC only (DOPC:cyt *c* = 200:1). (B, right panel) Tyrosine nitration yields of cyt *c* by PN under different conditions. (1) cyt *c* + PN; (2) cyt *c* + PN + CL (DOPC:CL:cyt *c* = 25:25:1); (3) cyt *c* + PN + CL (DOPC:CL:cyt *c* = 100:100:1); (4) cyt *c* + PN + DOPC (DOPN:cyt *c* = 200:1); (5−7) 1−3 with 1.2 mM CO_2, respectively.

Scheme 6. Manganese Porphyrin−Antioxidant Redox Couples as PN Decomposition Systems Modified from ref 55

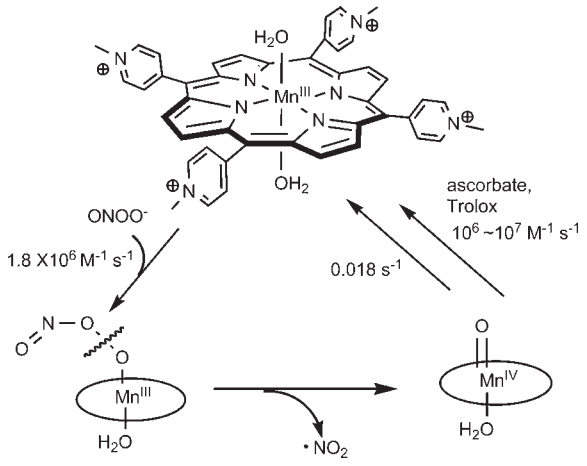

examined carefully by our group[55−57] and the Monsanto group.[128] Porphyrins bearing charged ligands, such as the cationic Mn- and FeTMPyP or the anionic sulfonate complexes, have been the focus of most PN decomposition catalyst studies. In this review, the reaction mechanisms of two representative metalloporphyrins with PN will be briefly discussed. Water-soluble manganese(III) porphyrins react rapidly with PN, forming a stable Mn^{IV}=O species and $\cdot NO_2$.[55] Unlike the proposed radical cage [Fe^{IV}=O$\cdot NO_2$] formed in metMb/PN interactions, the generated $\cdot NO_2$ does not rebound with Mn=O rapidly but diffuses into the solvent and nitrates exogenous substrates. In the meantime, this high-valent Mn^{IV}=O is reduced very slowly to Mn^{III}. However, the addition of biological antioxidants such as ascorbate and Trolox dramatically increased the turnover of PN decomposition through the reduction of Mn^{IV}=O, with a rate on the same order of magnitude as the formation of Mn^{IV}=O by PN (Scheme 6). Therefore, concurrent administration of reducing agents with manganese porphyrins may be an avenue for their pharmacological application.

Stern et al. have shown that [Fe^{III}TMPyP] and [Fe^{III}TMPS] display profound activity as "peroxynitrite isomerases",[128] converting $ONOO^-$ to NO_3^-. Lee et al. showed that Fe^{III}TMPyP reacts rapidly with $ONOO^-$ to afford OFe^{IV}TMPyP and $\cdot NO_2$.[56] In analogy to manganese porphyrins, this OFe^{IV}TMPyP appears to be relatively unreactive toward $\cdot NO_2$ and nitrite but can catalyze the conversion of excess $ONOO^-$ to NO_3^- with a rate constant of 1.8×10^6 M^{-1} s^{-1}. This represents a very significant advantage for the development of therapeutics based on this type of metallporphyrin reactivity because the protein nitration due to PN can be drastically reduced. Fe^{III}TMPS and PN interactions also involve the oxidation of Fe^{III}TMPS and give rise to an Fe^{IV}=O species, with concomitant formation of $\cdot NO_2$. Shimanovich et al. found that a fast rebound of NO_2 to Fe^{IV}=O accounts for a preferential pathway for the reduction of Fe^{IV}=O in the catalytic circle.[57] The presence of this "rebound" process sets Fe^{III}TMPS apart from manganese porphyrins in that it can catalytically and cleanly decompose PN to harmless products without the aid of additional reducing agents (Scheme 7). Surprisingly, Mn^{III} and Fe^{III}TMPyP are both able to efficiently catalyze the dismutation of the $ONOO^-$ precursor superoxide ($O_2^{\bullet -}$) into O_2 and H_2O_2.[55,56] Significantly, recent developments of a second-generation catalyst, based on Fe-2-TMPyP, led to the discovery of the highly reactive analogue FP-15.[129,130] In several studies, this compound has been shown to be capable of reducing myocardial infarct size and reactive hyperemia as well as other pathological conditions, including diabetic neuropathy.[129,131−133] These very promising developments are an excellent example of "unintended" favorable outcomes of basic research in bioinorganic chemistry that offer the promise of far-reaching impact in the health sciences.

The catalytic rate constants for PN decomposition by heme proteins and manganese/iron porphyrins are summarized in Table 1.

(128) Stern, M. K.; Jensen, M. P.; Kramer, K. *J. Am. Chem. Soc.* **1996**, *118*, 8735–8736.

(129) Mabley, J. G.; Liaudet, L.; Pacher, P.; Southan, G. J.; Groves, J. T.; Salzman, A. L.; Szabo, C. *Mol. Med.* **2002**, *8*, 581–590.

(130) Szabo, C.; Mabley, J. G.; Moeller, S. M.; Shimanovich, R.; Pacher, P.; Virag, L.; Soriano, F. G.; Van Duzer, J. H.; Williams, W.; Salzman, A. L.; Groves, J. T. *Mol. Med.* **2002**, *8*, 571–580.

(131) Radovits, T.; Seres, L.; Gero, D.; Lin, L. N.; Beller, C. J.; Chen, S. H.; Zotkina, J.; Berger, I.; Groves, J. T.; Szabo, C.; Szabo, G. *Mech. Ageing Dev.* **2007**, *128*, 173–181.

(132) Drel, V. R.; Pacher, P.; Vareniuk, I.; Pavlov, I. A.; Ilnytska, O.; Lyzogubov, V. V.; Bell, S. R.; Groves, J. T.; Obrosova, I. G. *Int. J. Mol. Med.* **2007**, *20*, 783–792.

(133) Drel, V. R.; Pacher, P.; Vareniuk, I.; Pavlov, I. A.; Ilnytska, O.; Lyzogubov, V. V.; Tibrewala, J.; Groves, J. T.; Obrosova, I. G. *Eur. J. Pharmacol.* **2007**, *569*, 48–58.

Scheme 7. Mechanism of PN Interactions with FeTMPS and FeTMPyP, Modified from References 55−57

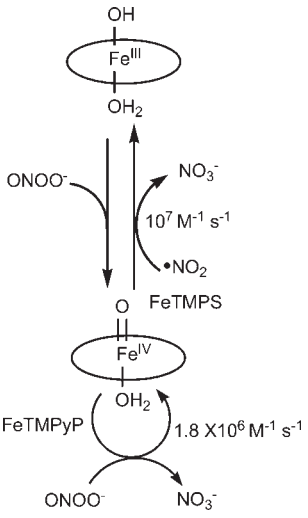

Table 1. Reaction of PN with Heme Proteins and Porphyrins (All pHs Are around pH 7.4)

protein/porphyrin	rate constant, M^{-1} s^{-1}	reference
oxyMb	5.4×10^4	134
metMb	1.0×10^4	45
oxyHb	8.8×10^4	134
myeloperoxidase	6.2×10^6	81
lactoperoxidase	3.3×10^5	81
chloroperoxidase	7.1×10^5	82
cytochrome c^{2+}	2.3×10^5	116
CL-bound cytochrome c^{3+} (L/P = 100)	5.0×10^3	this work
HRP	3.2×10^6	81
MP-11	$\sim 10^6$	80
cytochrome $P450_{NOR}$	$\sim 10^7$	79
cytochrome $P450_{BM3}$	$\sim 10^7$	80
NOS	2.2×10^5	135
MnTMPyP	3.2×10^6	55
FeTMPS	3.0×10^5	57
FeTMPyP	5.0×10^7	56
FP15	2.0×10^7	130
CO_2	3.4×10^4	136

Summary and Conclusions. Reactions of heme proteins with PN are complex, depending on the type of heme protein, the concentration of PN, and the specific reaction conditions. In biological systems, the level of CO_2 also has to be taken into account. Considering the bimolecular rate constants between heme proteins and PN as shown in Table 1, the presence of CO_2 at 1.2 mM definitely competes with oxyMb, oxyHb, or their ferric forms to react with PN, whereas the influence of CO_2 on P450s might not be as significant. The turnovers of histidine-ligated heme proteins by PN may all share the same Cpd II intermediate, which can arise from a precursor radical cage [Fe^{IV}=O·NO_2], as illustrated for Mb in Scheme 1. Upon concurrent liberation of the nitrating ·NO_2 (k_e), Cpd II can be observed distinctly. Meanwhile, the unreleased NO_2 may recombine or rebound to Cpd II and "collapse" into the Fe^{III} state and NO_3^- (k_r). Depending on the ratio of k_e/k_r, the catalytic effect of heme protein on PN-mediated nitration can be reversed; difficulty in trapping Cpd II during the reaction may also increase. The ratio of k_e/k_r is determined by the sequence and conformation of the protein as well as the configuration of the heme. Nonetheless, thiolate-ligated heme proteins such as CPO and P450 may also lead to ferric nitrosyls, as reported by Green et al.[87] Identification of heme protein/PN intermediates has generally been heavily dependent on stopped-flow UV−vis spectroscopy, and it is therefore prudent to examine and confirm those intermediates with additional techniques, such as kinetic criteria for diagnostic reactions, Mössbauer spectroscopy, X-ray absorption spectroscopies, etc. The understanding of these complex reactions between heme proteins and PN provides diverse avenues to the development of novel and powerful porphyrin-based therapeutics.

Experimental Section

Materials. Horse heart cytochrome *c* (type C-2506, >99%), butylated hydroxytoluene (BHT), and sodium hydroxide were purchased from Sigma. Hydrogen peroxide (30%) and perchloric acid (70%) were obtained from J. T. Baker. Diethylenetriaminepentaacetic acid (DTPA) was obtained from Alfa Aesar. Bovine heart cardiolipin (bhCL) and 1,2-dioleoyl-*sn*-glycero-3-phosphocholine (DOPC) were purchased from Avanti Polar Lipids Inc. Standard nitrotyrosine-containing peptide KY*IPGTLGK was custom-synthesized by Sigma Genosys.

Preparation of Vesicles. Small unilamellar vesicles were prepared by sonication as previously described.[137] Briefly, mixtures of bhCL and DOPC powders were dissolved in chloroform and transferred into 5 mL test tubes. Thin films of lipid were deposited on the walls of the test tubes after evaporation of the solvent with a stream of argon and were then left under high vacuum for 6 h. The dried lipid films were hydrated in a phosphate buffer (100 mM or 50 mM, 0.1 mM DTPA) at room temperature for 1 h. The hydrated bhCL/DOPC (1:1) or DOPC-containing lipid solutions were sonicated with a probe tip sonicator (Branson) in an ice−water bath for 5 min. After sonication, all samples were settled for 10 min. The vesicle suspensions were centrifuged at 12 000 rpm for 5 min to remove the sonicator tip debris. Minimal exposure of lipids to light was ensured throughout the above procedures.

Peroxynitrite (PN). PN was synthesized from hydrogen peroxide and nitrous acid as described[138] using a sp250i syringe pump (KD scientific). To avoid any contamination with bicarbonate from ambient air, all of the reagents for PN synthesis were degassed with argon thoroughly before mixing; the synthesized PN was later collected and kept under argon as well. Contaminating hydrogen peroxide was reduced to less than 5% (molar ratio) of PN by manganese dioxide (10 mg mL^{-1} at 4 °C for 15 min); MnO_2 was removed through a 0.2 μm membrane syringe filter (PALL). PN concentrations were determined at 302 nm (ε_{302} = 1670 M^{-1} cm^{-1}).[138] The nitrite and nitrate contents in PN were estimated by a Griess reagent and nitrate reductase purchased from Cayman. PN was decomposed in 0.14 M $HClO_4$ prior to the above assay in that 90% of PN

(134) Exner, M.; Herold, S. *Chem. Res. Toxicol.* **2000**, *13*, 287–293.
(135) Marechal, A.; Mattioli, T. A.; Stuehr, D. J.; Santolini, J. *J. Biol. Chem.* **2007**, *282*, 14101–14112.
(136) Denicola, A.; Freeman, B. A.; Trujillo, M.; Radi, R. *Arch. Biochem. Biophys.* **1996**, *333*, 49–58.
(137) Luo, M.; Fadeev, E. A.; Groves, J. T. *J. Am. Chem. Soc.* **2005**, *127*, 1726–1736.
(138) Koppenol, W. H.; Kissner, R.; Beckman, J. S. *Methods Enzymol.* **1996**, *269*, 296–302.
(139) Kakinoki, K.; Maeda, Y.; Hasegawa, K.; Kitano, H. *J. Colloid Interface Sci.* **1995**, *170*, 18–24.

decomposes into NO_3^- under acidic conditions. The concentrations of hydrogen peroxide in PN before and after manganese dioxide treatment were measured by a PeroXOquant Quantitative peroxide assay kit (Pierce Biotechnology) as instructed. The H_2O_2 measurements were performed after decomposition of PN at a neutral pH phosphate buffer (0.2 M, pH 7.2). PN solutions were prepared by dilution of the stock solution immediately before use with 0.01 M NaOH to achieve the required concentrations. All of the solutions involving the reactions with PN were purged with argon vigorously before mixing.

Cytochrome *c* Nitration. Nitration of cyt c^{3+} was performed by reaction with PN in the absence and presence of physiological concentrations of CO_2. To prepare pure cyt c^{3+}, a small amount of potassium ferricyanide (Sigma) was added to dissolved cyt *c* in a 0.1 M (pH 7.2) phosphate buffer to oxidize the remaining cyt c^{2+} in solution. The solution was subsequently purified chromatographically over an Econo-Pac 10DG column (Bio-Rad) using a 0.1 M phosphate buffer solution (pH 7.2) as the eluant. The concentration of cyt *c* was determined by measuring the absorbance at 340 nm (ε_{340} = 21.4 mM^{-1} cm^{-1}) and 550 (ε_{550} = 8 mM^{-1} cm^{-1}).[139]

To achieve efficient and reproducible nitration of cyt *c* by synthetic PN, cyt *c* and PN were mixed by a stopped-flow apparatus. Before CL-bound cyt *c* was reacted with PN, cyt *c* was incubated with bhCL/DOPC (1:1) or DOPC-only liposomes in a 100 mM phosphate buffer for 5 min while being purged with argon. The mixings were performed with varied amounts of PN basic solutions and cyt *c* with or without liposome solutions in a 100 mM phosphate buffer (pH 7.4, 0.1 mM DTPA). The nitrated cyt *c* solutions were collected at the outlet of the stopped-flow apparatus. A BHT solution (final concentration 50 μM) was added immediately into each resulting solution to quench any further radical reactions. The resulting solutions (200 μL) were subjected to protein dialysis with D-tube dialyzer (Calbiochem) against 50 mM ammonium biocarbonate (50 mM, pH 8) buffer for tyrpsin digestion and HPLC−tandem MS analysis.

Trypsin Digestion and LC−MS/MS Peptide Mapping. Control and PN-treated liposome-bound cyt *c* samples were digested with trypsin [1:1 (w/w), Promega] at 37 °C for 24 h. A known amount of nitrotryosine-containing peptide KY*IPGTLGK was spiked into the control solution after digestion to determine the time delay between UV−vis diode array detection and MS analysis. All of the digested samples were immediately analyzed by a ThermoFinnigan LCQ DECA XP Plus ion trap mass spectrometer equipped with a Surveyor PDA UV−vis detector. Digested samples were analyzed on a C-12 reverse-phase column (Jupiter, 4 μm, 150 × 2.00 mm, Phenomenex) using a gradient elution described as follows. The solvent system consisted of solvent A (0.15% trifluoroacetic acid, 5% acetonitrile, and H_2O) and solvent B (0.1% trifluoroacetic acid, 80% acetonitrile, and H_2O). The elution started with an isocratic elution with 2% B in the first 3 min followed by a linear gradient to 45% B over 57 min and to 98% over 4 min at a flow rate of 0.2 mL min^{-1}. The ESI conditions were recorded as follows: sheath gas, 90 arbitrary units; auxiliary gas, 30 arbitrary units; spray voltage, 3.5 kV; capillary temperature, 200 °C; capillary voltage, 45 V; tube lens offset, 25 V. Data were acquired in positive mode using the *Xcalibur* software package (Thermo) with a SEQUEST database search. Combining a SEQUEST search with manual evaluation, different nitrated peptides absorbing at 365 nm were identified unambiguously by tandem MS. The tyrosine nitration yields of cyt *c* under different conditions were computed by normalizing the total peak areas of nitrotyrosine peptides in the LC chromatogram to an intact peptide GITWK found in all of the chromatograms. The values of cyt *c* nitration yields in the presence of liposomes were calculated by comparing them with the total nitration yields of cyt *c* without liposomes estimated by HPLC-Q-TOF as described.[54]

Stopped-Flow Kinetic Analysis. Stopped-flow kinetic studies were carried out using a Hi-Tech SF-61DX2 double-mixing stopped-flow spectrophotometer (Hi-Tech, Salisburg, U.K.). The mixing time of the instrument is less than 2 ms, and the mixing cell is 1 cm long. The reactions were monitored either at a selected wavelength (single-wavelength mode) or by using a diode-array detector to record the entire visible range at each time point. For all of the studies of the reactions under CO_2-free conditions, the stopped-flow lines were washed with argon-purged doubly deionized water immediately before the experiments. Thoroughly degassed solutions of cyt *c*, liposome, and PN were transferred into Hamilton gastight syringes right before mixing. Several shots were collected as fast as possible. With all of these efforts, essentially no CO_2 was involved during the mixing of cyt *c* and PN. The traces were averaged from at least three shots. Kinetic data were analyzed and fitted on *KinetAsyst* software provided by Hi-Tech. Calculations and data treatment were performed using Microsoft Excel 2000 and a commercial graphics and data analysis software (*Origin 7.5*; MicroCal Inc.). In CO_2-involved experiments, ~2.5 mM HCO_3^- was premixed with liposomes followed by mixing with other reactants in open-air syringes by the stopped-flow apparatus.

HPLC-Chip-Q-TOF MS Analysis. Nitrated protein mixtures were thoroughly dialyzed (Slide-A-Lyzer mini dialysis units, 7000 MWCO, Pierce) against water prior to further analysis by an Agilent 6510 LC-Q-TOF MS. This Q-TOF was coupled with an Agilent HPLC-chip (G4240-62001, Zorbax 300SB-C18) for sample loading and separation. The LC-chip solvents were 0.1% formic acid/3% acetonitrile/97% H_2O (v/v/v; solvent A) and 0.1% formic acid/10% H_2O/90% acetonitrile (v/v/v; solvent B). Protein samples were diluted in solvent A before injection. The online LC-chip separation employed a gradient from 3 to 90% solvent B in 6 min and then from 90 to 100% B in 8−10 min, followed by 100% B for 5 min. The flow rate was 0.5 μL min^{-1}. Proteins eluted from the HPLC-chip were directly injected into the coupled Q-TOF MS with a nanoelectrospray ionization source. MS data were acquired and processed using an Agilent Masshunter workstation and the included qualitative analysis software.

Acknowledgment. We are grateful for support of this research by the National Institutes of Health (Grant 2R37 GM036298).